Supplementary Information

Tracking Fast Cellular Membrane Dynamics with Sub-nm Accuracy in Normal Direction

Hui Yu[†a], *Yuting Yang*[a], *Yunze Yang*[b], *Fenni Zhang*[b], *Shaopeng Wang*[b], *Nongjian Tao*[†b,c]

[a] Institute for Personalized Medicine, School of Biomedical Engineering, Shanghai Jiao Tong University, Shanghai 200030, China

[b] Biodesign Center for Bioelectronics and Biosensors, Arizona State University, Tempe, AZ 85287, USA

[c] State Key Laboratory of Analytical Chemistry for Life Science, School of Chemistry and Chemical Engineering, Nanjing University, Nanjing 210093, China

*Correspondence should be sent to

Prof. Hui Yu: hui.yu@sjtu.edu.cn; +86-21-62932274

Address: 1954 Huashan Road, Med-X Institute #416, Shanghai, 200240 China;

or Prof. Nongjian Tao: njtao@asu.edu; +1- (480)-965-4456

Address: 1001 S. McAllister Ave., Tempe, AZ, 85287, US

Displacement measurement from recorded videos

The displacement was measured with a differential detection algorithm, which expresses the displacement from $\Delta d = \alpha \frac{I_A - I_B}{I_A + I_B}$, where I_A and I_B are intensities of the two halves of a region of interest (ROI) shown in the inset of Fig. S1, and α is calibration factor. To determine α, we translated the sample stage over known distances, and determined the corresponding $\frac{I_A - I_B}{I_A + I_B}$. The results are plotted in Fig.S1, showing that $\frac{I_A - I_B}{I_A + I_B}$ changes linearly with Δd within a displacement range of ~200 nm. This displacement range is sufficient for measuring cellular membrane fluctuations, which are typically smaller than a few nm. The slope of the linear relation was extracted, giving $1/\alpha$. Note that beyond the 200 nm displacement range, the calibration curve we got differs from those reported in weak optical tweezers experiments because part of the particle image falls out of the field of view.

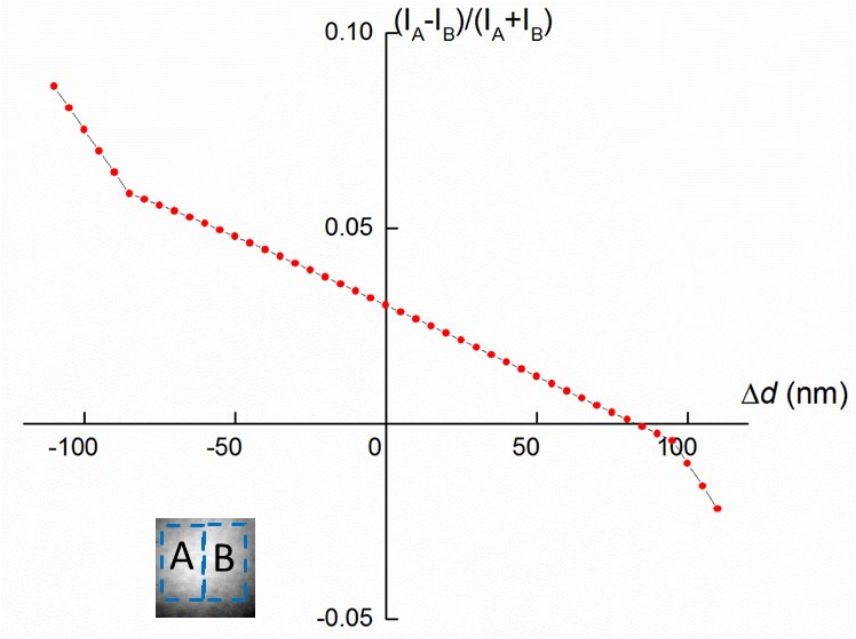

Fig. S1 Calibration of differential detection algorithm for tracking membrane fluctuations. Example shown here is for a 1-μm polystyrene particle (image shown in inset).

Differential measurement strategy to remove low frequency common noise

To remove the low frequency system noise, we adopted a differential measurement strategy as shown in Fig.S2. The particle or membrane image was separated into two sub-images, each containing half of the particle or membrane. The displacements of the two sub-

particle/membrane were calculated using the algorithm described above, with $\Delta d_1 = \alpha_1 \frac{I_{A1} - I_{B1}}{I_{A1} + I_{B1}}$ and $\Delta d_2 = \alpha_2 \frac{I_{A2} - I_{B2}}{I_{A2} + I_{B2}}$, and α_1 and α_2 were calibrated separately. The finial differential displacement was $\Delta d = \Delta d_1 - \Delta d_2$.

Fig.S2 Differential measurement strategy

Shot noise analysis

To verify that the high frequency noise is dominated by shot noise, we varied illumination intensity and examined the noise dependence on the illumination intensity (Fig.S3). The power spectral density (PSD) shows that the illumination intensity mainly affects the high frequency noise (left, Fig. S2). The noise level (integrated from 1 kHz to 50 kHz) is inversely proportional to the square root of the total number of photons (*N*) which is expected for shot noise (right of Fig. S2). We also examined the noise dependence on the number of pixels in a given ROI for a given illumination intensity (Fig. S4). As expected, the high frequency noise decreases with the number of pixels (left of Fig. S3) used as the ROI, and the noise level (integrated from 1 kHz to 50 kHz) is inversely proportional to the square root of the total number of pixels (N_p). This is because the total number of photons at a fixed illumination is proportional to the number of pixels.

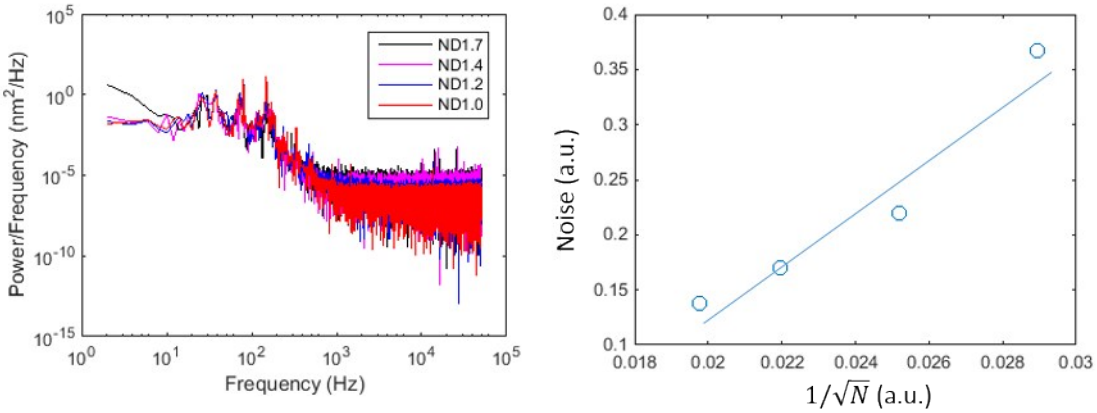

Fig. S3 Dependence of noise on illumination intensity. (Left) PSD at different illumination intensities adjusted by neutral density (ND) optical filters. The fractions of transmittance are 0.02, 0.04, 0.06 and 0.09 for ND=1.7, 1.4, 1.2 and 1.0, respectively. (Right) Noise level dependence on the number of photons.

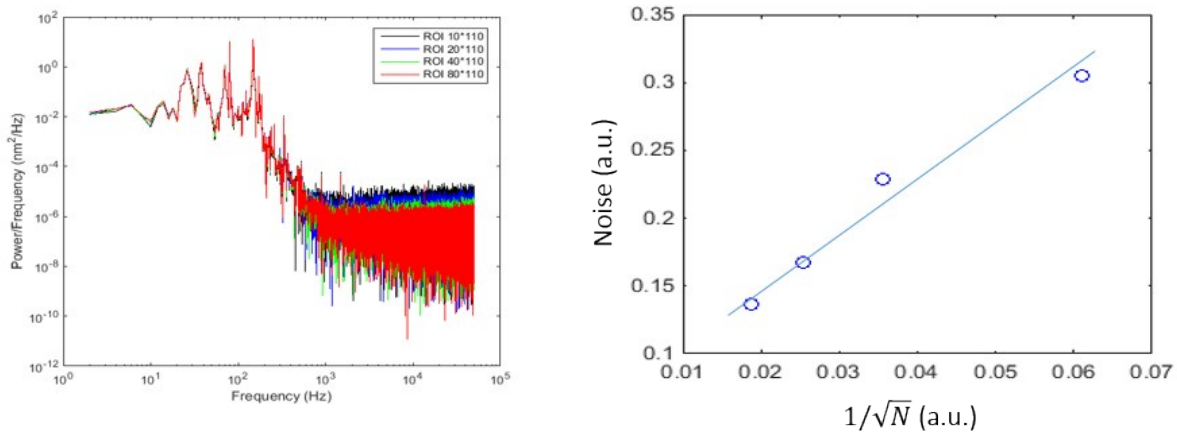

Fig. S4 Dependence of noise on number of pixels for a given ROI. (Left) PSDs of a ROI with different numbers of pixels. (Right) Noise level dependence on the number of photons for a given ROI.

Membrane fluctuation of HEK 293 cells was not resolvable without the differential measurement strategy at slow timescale.

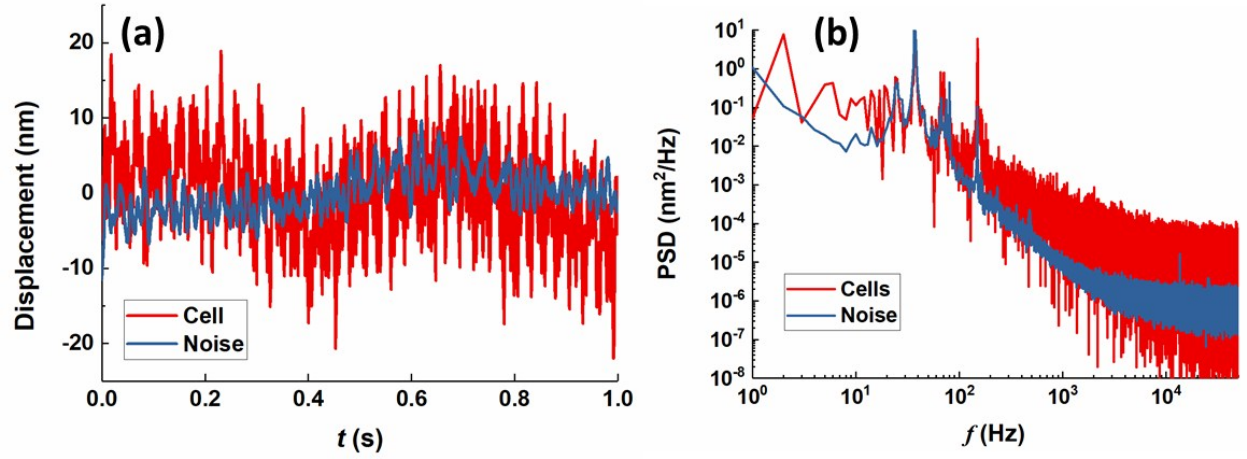

Fig. S5 Membrane fluctuations of a HEK-293 cell measured with the single point detection. (a) Time traces of membrane fluctuations (red) and system noise (blue). (b) PSDs of the corresponding membrane fluctuations (red) and noise (blue). Note that the system noise was determined from a 1-μm polystyrene particle attached a glass coverslip.

Hydrodynamic model.

The model below is based on the Helfrich analysis [1] that has been widely used for studying cellular membrane fluctuations [2-5](2-4). The energy of a planar membrane fluctuation is described by a free energy functional

$$F = \int dS\left[\frac{1}{2}\sigma(\nabla h)^2 + \frac{1}{2}\kappa\left(\nabla^2 h\right)^2\right] \qquad \text{(S1)}$$

where *h* is the displacement of membrane from its equilibrium position, κ is the bending modulus, σ is the surface tension, and the integral sums over the whole surface. Using the equipartition theorem, the auto-correlation function of the fluctuation is

$$\left\langle {h_q}^2 \right\rangle = \frac{k_B T}{\kappa q^4 + \sigma q^2} \quad ; \qquad \text{(S2)}$$

where q is the wave number of a membrane fluctuation mode, k_B is the Boltzmann constant, and T is temperature. The temporal height-height correlation function for a bilayer is

$$\left\langle h_q(t) h_q(0) \right\rangle = \frac{k_B T}{\kappa q^4 + \sigma q^2} e^{-\gamma(q)t} \qquad \text{(S3)}$$

where $\gamma(q)$ is the relaxation rate given by,

$$\gamma(q) = (\kappa q^3 + \sigma q)/4\eta \qquad \text{(S4)}$$

for a free bilayer, where η is the mean viscosity of the two fluids separated by the membrane. According to Wierner-Khinching theorem, PSD is determined from the Fourier transform of the autocorrelation function,

$$PSD_1(\omega,r) = \int \frac{d^2 q}{(2\pi)^2} \int \left\langle h_q(t) h_q(0) \right\rangle e^{-i\omega t} dt \quad . \qquad \text{(S5)}$$

Substituting Eq. S3 into Eq. S5, and transforming it into polar coordinates, the PSD of single point detection is given by,

$$PSD_1(\omega,r) = \int_0^{2\pi} d\theta \int_0^{+\infty} \frac{q dq}{(2\pi)^2} \frac{k_B T}{\kappa q^4 + \sigma q^2} \int e^{-\gamma(q)t} e^{-i\omega t} dt$$

$$= \frac{k_B T}{\pi} \int_0^{+\infty} \frac{1}{\kappa q^3 + \sigma q \gamma^2 + \omega^2} \frac{\gamma}{} dq \quad . \qquad \text{(S6)}$$

For differential measurement, we consider displacement difference between two adjacent locations along the cell edge,

$$\Delta h(r_1,r_2,t) = h(r_1,t) - h(r_2,t). \quad \text{(S7)}$$

For each ***q***-mode, a phase difference $q.(r - r')$ exists, which allows us to express Eq. S7 as,

$$\Delta h_q(r_1,r_2,t) = h_q(r_1,t) - h_q(r_2,t) = h_q(r_1,t)\left(1 - e^{iq(r-r')}\right), \quad \text{(S8)}$$

and the autocorrelation function is

$$\left\langle \Delta h_q(r,r',t)\Delta h_q(r,r',0)\right\rangle = \left\langle h_q(t)h_q(0)\right\rangle\left(2 - 2e^{iq(r-r')}\right). \quad \text{(S9)}$$

Fourier transform of Eq. S9 leads to PSD for the two-point detection algorithm, given by

$$PSD_2(\omega,r_1,r_2) = \int \frac{d^2q}{(2\pi)^2}\int \left\langle \Delta h_q(r,r',t)\Delta h_q(r,r',0)\right\rangle e^{-i\omega t}dt \quad \text{(S10)}$$

Substituting Eq. S9 into Eq. S10, and transforming it into polar coordinates, we obtain the PSD of two-point detection,

$$PSD_2(\omega,r_1,r_2) = \frac{k_BT}{\pi}\int_0^{+\infty} \frac{H(q)}{\kappa q^3 + \sigma q\gamma^2 + \omega^2}\frac{\gamma}{}dq \quad \text{(S11)}$$

where

$$H(q) = \frac{2}{\pi}\int_0^{\pi}\left(1 - \cos\left(q|r_1 - r_2|\cos\theta\right)\right)d\theta \quad \text{(S12)}$$

1. Frequency scaling laws of membrane fluctuations

Free bilayer membrane.

For a free bilayer, $\gamma(q) = (\kappa q^3 + \sigma q)/4\eta$, and we have (Eqs. S11 and 12),

$$PSD_2(\omega,r_1,r_2) = \frac{k_BT}{2\eta\pi^2}\int_0^{+\infty}\int_0^{\pi}\frac{\left(1 - \cos\left(q|r_1 - r_2|\cos\theta\right)\right)}{\left((\kappa q^3 + \sigma q)/4\eta\right)^2 + \omega^2}dqd\theta \quad \text{(S13)}$$

At high frequencies, bending modulus dominates, such that $\kappa q^3 \gg \sigma q$, we obtain

$$PSD_2(\omega,r_1,r_2)=\frac{k_BT}{2\eta\pi^2}\int_0^{+\infty}\int_0^{\pi}\frac{\left(1-\cos\left(q|r_1-r_2|\cos\theta\right)\right)}{\left(\kappa q^3/4\eta\right)^2+\omega^2}dqd\theta \quad . \tag{S14}$$

We define a characteristic length,

$$\lambda_\omega=\left(\frac{\kappa}{4\eta\omega}\right)^{1/3}. \tag{S15}$$

Substituting $q'=\lambda_\omega q$ into Eq. S14 leads to

$$PSD_2(\omega,r_1,r_2)=\frac{k_BT}{2\eta\pi^2\omega^2\lambda_\omega}\int_0^{+\infty}\int_0^{\pi}\frac{1-\cos\left(\frac{|r_1-r_2|}{\lambda_\omega}q'\cos\theta\right)}{1+q'^6}d\theta dq'$$

$$=\frac{k_BT}{\pi^2\left(2\kappa\eta^2\right)^{1/3}\omega^{5/3}}\int_0^{+\infty}\int_0^{\pi}\frac{1-\cos\left(\frac{|r_1-r_2|}{\lambda_\omega}q'\cos\theta\right)}{1+q'^6}d\theta dq' \quad . \tag{S16}$$

For single point detection, the high frequency limit of the PSD is

$$PSD_1(\omega,r)\sim\frac{k_BT}{6\pi\left(2\kappa\eta^2\right)^{1/3}\omega^{5/3}}. \tag{S17}$$

$PSD_2(\omega,r_1,r_2)$ is a homogenous function and can be written as

$$PSD_2(\omega,r_1,r_2)\sim PSD_1(\omega,r)f\left(\frac{|r_1-r_2|}{\lambda_\omega}\right) \tag{S18}$$

where

$$f\left(\frac{|r_1-r_2|}{\lambda_\omega}\right)=\frac{6}{\pi}\int_0^{+\infty}\int_0^{\pi}\frac{1-\cos\left(\frac{|r_1-r_2|}{\lambda_\omega}q'\cos\theta\right)}{1+q'^6}d\theta dq' \tag{S19}$$

is a universal function of the ratio $\frac{|r_1-r_2|}{\lambda_\omega}$.

Fig. S6 plots $f\left(\frac{|r_1 - r_2|}{\lambda_\omega}\right)$ vs. $\frac{|r_1 - r_2|}{\lambda_\omega}$, showing an increase and then reach a plateau at large $|r_1 - r_2|/\lambda_\omega$ (corresponding to high ω for a given $|r_1 - r_2|$). Thus, according to Eq. S18, we expect that the two-point PSD follow the same scaling law at the single-point PSD or $PSD_2(\omega, r_1, r_2) \sim \omega^{-5/3}$ at high frequencies.

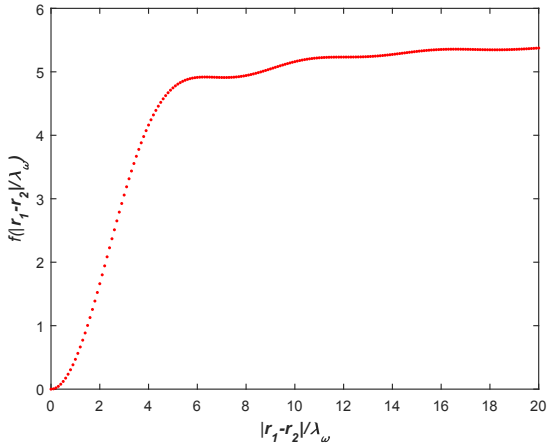

Fig. S6 Numerical calculation of $f\left(\frac{|r_1 - r_2|}{\lambda_\omega}\right)$ vs. $\frac{|r_1 - r_2|}{\lambda_\omega}$.

Membrane near a rigid wall.

For cells with cytoskeletons to support the membrane structure, the free membrane assumption is no longer appropriate. A better approach is to assume that the membrane is constrained with a rigid wall at a distance D (the spacing between cytoskeleton and membrane). In this case, the relaxation rate is given by according to a hydrodynamic theory[5, 6],

$$\gamma(q) = \kappa_q q^4 \Lambda(q) \qquad \text{(S20)}$$

where

$$\Lambda(q) = -\frac{e^{-2Dq}}{4\eta q}\left(1 - e^{2Dq} + 2Dq + 2(Dq)^2\right). \qquad \text{(S21)}$$

For wave numbers $q \ll 1/D$, which is the range achievable experimentally, by Tailor expansion, we have

$$\gamma(q) \to \frac{\kappa_q q^6 D^3}{3\eta}. \qquad \text{(S22)}$$

This leads to the modification of Eq. S17, 18 (4,6) as,

$$PSD_1(\omega,r) \propto \omega^{-4/3}. \quad \text{(S23)}$$

Similar to the derivation of Eq. S18, we have

$$PSD_2(\omega,r_1,r_2) = PSD_1(\omega,r) \cdot g\left(\frac{|r_1 - r_2|}{\lambda'_\omega}\right) \quad \text{(S24)}$$

where $\lambda'_\omega = \left(\frac{\kappa D^3}{24\eta\omega}\right)^{1/6}$ is a characteristic length, and $g\left(\frac{|r_1 - r_2|}{\lambda_\omega}\right)$ is a universal function of $\frac{|r_1 - r_2|}{\lambda'_\omega}$. $g\left(\frac{|r_1 - r_2|}{\lambda_\omega}\right)$ is similar to $f\left(\frac{|r_1 - r_2|}{\lambda'_\omega}\right)$, we thus conclude $PSD_2(\omega,r_1,r_2) \sim \omega^{-4/3}$.

References

1. W. Helfrich, *Zeitschrift für Naturforschung C*, 1973, **28**, 693-703.
2. T. Betz, M. Lenz, J.-F. Joanny and C. Sykes, *Proceedings of the National Academy of Sciences*, 2009, **106**, 15320-15325.
3. T. Betz and C. Sykes, *Soft Matter*, 2012, **8**, 5317-5326.
4. N. Gov, A. G. Zilman and S. Safran, *Physical Review E*, 2004, **70**, 011104.
5. N. Gov, A. Zilman and S. Safran, *Physical review letters*, 2003, **90**, 228101.
6. F. Brochard and J. Lennon, *Journal de Physique*, 1975, **36**, 1035-1047.